Stability diagram for dense suspensions of model colloidal Al2O3 particles in shear flow

Please check the document version of this publication:

• A submitted manuscript is the version of the article upon submission and before peer-review. There can be important differences between the submitted version and the official published version of record. People interested in the research are advised to contact the author for the final version of the publication, or visit the DOI to the publisher's website.
• The final author version and the galley proof are versions of the publication after peer review.
• The final published version features the final layout of the paper including the volume, issue and page numbers.

Link to publication

Stability diagram for dense suspensions of model colloidal Al$_2$O$_3$ particles in shear flow

Martin Hecht,[1] Jens Harting,[1] and Hans J. Herrmann[2,3]

[1]*Institute for Computational Physics, Pfaffenwaldring 27, D-70569 Stuttgart, Germany*
[2]*Computational Physics, IFB, Schafmattstraße 6, ETH Zürich, CH-8093 Zürich, Switzerland*
[3]*Departamento de Física, Universidade Federal do Ceará Campus do Pici, 60451-970 Fortaleza CE, Brazil*

In Al$_2$O$_3$ suspensions, depending on the experimental conditions, very different microstructures can be found, comprising fluidlike suspensions, a repulsive structure, and a clustered microstructure. For technical processing in ceramics, the knowledge of the microstructure is of importance, since it essentially determines the stability of a workpiece to be produced. To enlighten this topic, we investigate these suspensions under shear by means of simulations. We observe cluster formation on two different length scales: the distance of nearest neighbors and on the length scale of the system size. We find that the clustering behavior does not depend on the length scale of observation. If interparticle interactions are not attractive the particles form layers in the shear flow. The results are summarized in a stability diagram.

I. INTRODUCTION

Colloid science is a very fascinating research field, gaining more and more importance in the last years. It closely connects physics, chemistry, material science, biology, and several branches of engineering technology. According to its key role in modern science a considerable amount of research has been performed to describe colloidal suspensions from a theoretical point of view and by simulations [1–6] as well as to understand the particle-particle interactions [7–12], the phase behavior [13–16], the relevant processes on the microscale, and their influence on macroscopic parameters [17–19]. Colloidal suspensions are in fact complicated systems, since different time and length scales are involved. The particle sizes are on a mesoscopic length scale, i.e., in the range of nanometers up to micrometers. In systems of particles sized on this length scale Brownian motion often cannot be neglected. Depending on the particle sizes, materials, and concentrations, different interactions are of relevance and often several of them are in a subtle interplay: electrostatic repulsion, depletion forces, van der Waals attraction, hydrodynamic interaction, and Brownian motion are the most important influences. The properties of the suspension are strongly depending on the balance of the microscopic forces between the particles. Especially for industrial processes, where one needs to optimize certain material properties a detailed understanding of the relevant influences is needed. The stability of different microstructures and especially the clustering process are key properties which are of interest.

In our work we investigate these properties, focusing on Al$_2$O$_3$ particles of diameter 0.37 μm suspended in water. This is a widely used material in ceramics [20,21]. We have developed a simulation code for a Brownian suspension [22] and have adjusted the simulation parameters so that the simulation corresponds quantitatively to a real suspension such that experimental data can be compared directly. The diffusion coefficient, sedimentation velocity [22], and the viscosity of the suspension can be reproduced [23]. We also have tested the influence of polydispersity and found that its

influence on the results is small. It is much more important to choose the correct mean size of the particles [23]. For Al$_2$O$_3$ suspensions attractive van der Waals forces are important for the behavior of this material. Electrostatic repulsion of the charged particles counteracts the attraction and can prevent clustering depending on the particle surface charge. In Ref. [23] we have presented how one can relate parameters of Derjaguin-Landau-Vervey-Overbeek (DLVO) potentials [7,8] with experimental conditions. In the experiment one can control the pH value and the salt concentration. The latter can be expressed by the ionic strength I, which is an effective concentration of all ions present in the solution. Both the pH value and the ionic strength influence the charge of the colloidal particles. We have shown that for not too strongly attractive forces one can obtain reasonable quantitative agreement with experimental results: by adjusting the lubrication force, which represents the short range hydrodynamics, we are able to reproduce rheological data of a real suspension [23].

Three regimes can be identified and plotted in a stability diagram [23], which we want to investigate here in more detail: a clustered regime, in which particles aggregate to clusters, a fluidlike and stable suspension, and a repulsive region, for which the microstructure is similar to the ones known from glassy systems. From our previous work we know that our model works well, even quantitatively, in the suspended regime of the stability diagram and close to the borders between the different microstructures. In this paper we extend our investigations to different pH values, deeper in the clustered regime, and to the repulsive structure. We expect to gain insight to the microscopic structure on a qualitative level.

On these grounds we have explored the stability diagram of Al$_2$O$_3$ suspensions. The particles are uncharged close to the so called "isoelectric point" at pH=8.7. There, for all ionic strengths, the particles form clusters. For lower pH values particles can be stabilized in solution, because they are charged. For low pH values, low salt concentrations, and high volume fractions a repulsive structure can be found.

In the following section we shortly describe our simulation method. After that we discuss the criteria we apply to

characterize the microstructures. We utilize the pair correlation function and the structure factor to characterize the clustering behavior. Both of them in principle contain the same information, but we concentrate on certain peaks in either of them. Each peak in the correlation function and in the structure factor corresponds to a certain length scale and we chose either the correlation function or the structure factor, depending on which of the two quantities is more suitable under numerical criterions to observe on a given length scale. In the section thereafter we describe our simulation setup. In the results section we start with the discussion of the correlation function and the structure factor. Additionally, we evaluate the so-called demixing parameter Ψ [24]. To characterize the repulsive region we evaluate the mean squared displacement (MSD), which shows a plateau, if the particle motion consists of different processes acting on well separated time scales. Finally, the results are summarized in a stability diagram for our Al_2O_3 suspension. It shows the behavior of the suspension in an intuitive way and helps to design industrial processes using this material.

II. SIMULATION METHOD

Our simulation method consists of two parts: a molecular dynamics (MD) code, which treats the colloidal particles, and a stochastic rotation dynamics (SRD) simulation for the fluid solvent.

In the MD part of our simulation the colloidal particles are represented by monodisperse spheres. We include effective electrostatic interactions and van der Waals attraction, known as DLVO potentials [7,8], a lubrication force, and Hertzian contact forces. DLVO potentials are composed of two terms, the first one being an exponentially screened Coulomb potential due to the surface charge of the suspended particles

$$V_{Coul} = \pi \varepsilon_r \varepsilon_0 \left[\frac{2 + \kappa d}{1 + \kappa d} \frac{4 k_B T}{ze} \tanh \left(\frac{ze\zeta}{4 k_B T} \right) \right]^2$$
$$\times \frac{d^2}{r} \exp(-\kappa[r-d]), \qquad (1)$$

where d denotes the particle diameter and r is the distance between the particle centers. e is the elementary charge, T is the temperature, k_B is the Boltzmann constant, and z is the valency of the ions of added salt. ε_0 is the permittivity of the vacuum, $\varepsilon_r = 81$ is the relative dielectric constant of the solvent. κ is the inverse Debye length defined by $\kappa^2 = 8 \pi \ell_B I$, with the ionic strength I and the Bjerrum length $\ell_B = 7$ Å. The first fraction in Eq. (1) is a correction to the DLVO potential (in the form used in Ref. [25]), which takes the surface curvature into account and is valid for spherical particles [26].

The effective surface potential ζ is the electrostatic potential at the border between the diffuse layer and the compact layer. Smoluchowski related it to the electrokinetic mobility of the particle as $\mu = \zeta \varepsilon_0 \varepsilon_r / \eta$ [27]. The ζ potential can be related to the pH value of the solvent with a so-called $2pK$ charge regulation model [23].

The Coulomb term competes with the second part of the DLVO potential which is given by the attractive van der Waals interaction

$$V_{VdW} = \frac{A_H}{12} \left[\frac{d^2}{r^2 - d^2} + \frac{d^2}{r^2} + 2 \ln \left(\frac{r^2 - d^2}{r^2} \right) \right]. \qquad (2)$$

$A_H = 4.76 \times 10^{-20}$ J is the Hamaker constant [25]. The DLVO potentials exhibit two minima, one primary minimum, where the particles touch each other. Equation (2) diverges where in reality the primary minimum of the potential is located. Therefore we model the primary minimum by cutting off the DLVO potentials for small separations and substituting them by a parabola which is connected in a continuously differentiable manner to the DLVO potential. This cutoff is made at distances of several nanometers, where the potential has already reached negative values, i.e., where the potential descends to the primary minimum. The primary minimum is separated by a potential barrier from the secondary minimum, which occurs at larger particle distances and which is less deep. For low salt concentrations, i.e., large Debye screening lengths, the electrostatic repulsion overcompensates the van der Waals attraction and the secondary minimum disappears.

Long range hydrodynamic interactions are taken into account in the simulation for the fluid as described below. This can only reproduce interactions correctly down to a certain length scale. On shorter distances, a lubrication force has to be introduced explicitly in the molecular dynamics simulation:

$$\mathbf{F}_{lub} = -\mathbf{v}_{rel,\perp} \frac{6 \pi \eta}{r - d} \left(\frac{d}{4} \right)^2, \qquad (3)$$

with the relative velocity $\mathbf{v}_{rel,\perp}$ projected on the connecting line of the particle centers. η is the dynamic viscosity of the fluid. Our implementation of the interaction contains cutoff radii to connect it to the long-range hydrodynamics and to avoid numerical instability for particles touching each other [22,23].

To avoid that the particles penetrate each other, we are using a Hertz force described by the potential

$$V_{Hertz} = K(d-r)^{5/2} \quad \text{if } r < d, \qquad (4)$$

where K is an interaction constant and additionally a damping term

$$\mathbf{F}_{Damp} = -\mathbf{v}_{rel,\perp} \beta \sqrt{d-r}, \qquad (5)$$

with a damping constant β. For the integration of the translational motion we utilize a velocity Verlet algorithm [28].

For the simulation of a fluid solvent, many different simulation methods have been proposed: Stokesian dynamics (SD) [3,29,30], accelerated Stokesian dynamics (ASD) [31,32], pair drag simulations [4], Brownian dynamics (BD) [25,33], lattice Boltzmann (LB) [1,2,34,35], and stochastic rotation dynamics (SRD) [22,36,37]. These mesoscopic fluid simulation methods have in common that they make certain approximations to reduce the computational effort. Some of them include thermal noise intrinsically, or it can be included consistently. They scale differently with the number of em-

bedded particles and the complexity of the algorithm differs largely.

We apply the stochastic rotation dynamics method (SRD) introduced by Malevanets and Kapral [38,39]. It intrinsically contains fluctuations, is easy to implement, and has been shown to be well suitable for simulations of colloidal and polymer suspensions [22,23,36,37,40–42] and very recently for star polymers in shear flow [43]. The method is also known as "real-coded lattice gas" [36] or as "multiparticle-collision dynamics" (MPCD) [44]. It is based on so-called fluid particles with continuous positions and velocities. A streaming step and an interaction step are performed alternately. In the streaming step, each particle i is moved according to

$$\mathbf{r}_i(t + \tau) = \mathbf{r}_i(t) + \tau \mathbf{v}_i(t), \tag{6}$$

where $\mathbf{r}_i(t)$ denotes the position of the particle i at time t and τ is the time step. In the interaction step the fluid particles are sorted into cubic cells of a regular lattice and only the particles within the same cell interact among each other according to an artificial interaction. The interaction step is designed to exchange momentum among the particles, but at the same time to conserve total energy and total momentum within each cell, and to be very simple, i.e., computationally cheap: each cell j is treated independently. First, the mean velocity $\mathbf{u}_j(t') = \frac{1}{N_j(t')} \Sigma_{i=1}^{N_j(t')} \mathbf{v}_i(t)$ is calculated. $N_j(t')$ is the number of fluid particles contained in cell j at time $t' = t + \tau$. Then, the velocities of each fluid particle in cell j are rotated according to

$$\mathbf{v}_i(t + \tau) = \mathbf{u}_j(t') + \Omega_j(t') \cdot [\mathbf{v}_i(t) - \mathbf{u}_j(t')]. \tag{7}$$

$\Omega_j(t')$ is a rotation matrix, which is independently chosen at random for each time step and each cell. We use rotations about one of the coordinate axes by an angle $\pm \alpha$, with α fixed. The coordinate axis as well as the sign of the rotation are chosen at random, resulting in six possible rotation matrices. To remove anomalies introduced by the regular grid, one can either choose a mean free path of the order of the cell size or shift the whole grid by a random vector once per SRD time step as proposed by Ihle and Kroll [45,46].

Three different methods to couple the SRD and the MD simulation have been introduced in the literature. Inoue *et al.* proposed a way to implement no slip boundary conditions on the particle surface [36]. Padding and Louis very recently came up with full slip boundaries, where the fluid particles interact via Lennard-Jones potentials with the colloidal particles [47]. Falck *et al.* [48] have developed a "more coarse grained" method which we use for the simulations of the present paper and which we descibe shortly in the following.

To couple the colloidal particles to the fluid, the colloidal particles are sorted into the SRD cells and their velocities are included in the rotation step. One has to use the mass of each particle—colloidal or fluid particle—as a weight factor when calculating the mean velocity

$$\mathbf{u}_j(t') = \frac{1}{M_j(t')} \sum_{i=1}^{N_j(t')} \mathbf{v}_i(t) m_i, \tag{8}$$

with

$$M_j(t') = \sum_{i=1}^{N_j(t')} m_i, \tag{9}$$

where we sum over all colloidal and fluid particles in the cell, so that $N_j(t')$ is the total number of both particles, fluid plus colloidal ones. m_k is the mass of the particle with index i and $M_j(t')$ gives the total mass contained in cell j at time $t' = t + \tau$. In summary, the algorithm for the fluid simulation is described by Eqs. (6)–(9). To some of our simulations we apply shear. This is realized by explicitly setting the mean velocity $\mathbf{u}_j$ to the shear velocity in the cells close to the border of the system. Both colloidal and fluid particles are involved in this additional step. A thermostat is applied to remove the energy introduced to the system by the shear force. We have described the simulation method in more detail in Refs. [22,23].

III. BACKGROUND

In this paper we examine the microstructures obtained in our simulations for different conditions. We vary the pH value and the ionic strength I. The shear rate $\dot{\gamma}$ as an external influence is varied as well. We classify the microstructures in three categories: suspended, clustered, and repulsive. In the suspended case, the particles can move freely in the fluid and do not form stable clusters. In the clustered regime the particles form clusters due to attractive van der Waals forces. These clusters can be torn apart if shear is applied. In some of our simulations the clusters are very weakly connected and at small shear rates they are not only broken up into smaller pieces, but they dissolve to freely moving individual particles. In this case, we assign the microstructure to the suspended region, although in complete absence of the shear flow clusters are formed. At the borders between the different regimes in fact no sharp transitions can be observed. The DLVO forces rather steadily increase and compete with the hydrodynamic interactions. Accordingly, in experiments one cannot observe a sudden solidification, but a steadily increasing viscosity when leaving the suspended regime [23].

Similarly as for attractive forces, repulsive interactions can restrict the mobility of the particles. If this happens, the mean squared displacement of the particles shows a pronounced plateau, as it can be found in glassy systems. However, we speak of a "repulsive structure," because the change of the viscosity is not as strong as in glasses, where it often changes by many orders of magnitude, when the glass transition is approached. In addition, to claim that a system shows a glassy behavior would require one to investigate the temperature dependence of a typical time (e.g., particle diffusion time) and to show its divergence as the glass temperature is approached. This is difficult to do in the framework of our simulation model [22] and therefore we prefer to speak about a "repulsive structure" which might be identified as a colloidal glass in future work.

In this paper we would like to emphasize the analysis of the microstructure for different conditions. Our aim is to reproduce a so-called stability diagram by simulations. The stability diagram depicts the respective microstructure depending on the pH value and the ionic strength I. We apply different numerical tools to analyze the microstructure in our simulations and finally arrive at a stability diagram shown in Fig. 10, which summarizes the results which we present in the following sections.

The first tool we apply for that is the pair correlation function

$$g(r) = \frac{V}{N^2} \left\langle \sum_i \sum_{j \neq i} \delta(r - r_{ij}) \right\rangle \quad (10)$$

(see Ref. [28], p. 55), where V is the volume, N is the number of particles, and r_{ij} is the distance of two particles i and j; this can be used for a first characterization of the system. It shows maxima at certain typical particle distances, e.g., there is a nearest neighbor peak, and more complicated structures at larger distances, which we have assigned to typical particle configurations for small distances [22]. Here, we use the next-neighbor peak to analyze our data, which provides information of the short-range structure of the suspension. To observe the long-range structure we move on to its complementary quantity: the structure factor, defined by

$$S(\mathbf{k}) = \frac{1}{N} \sum_{l,m=1}^{N} \exp(i\mathbf{k} \cdot \mathbf{r}_{lm}), \quad (11)$$

where N is the number of particles, and $\mathbf{r}_{lm}$ is the vector from particle l to particle m. i denotes the imaginary unit here. The structure factor is defined in $\mathbf{k}$ space and it is related to the pair correlation function in real space by a three dimensional Fourier transform:

$$S(k) - 1 = \int d\mathbf{r} \exp(i\mathbf{k} \cdot \mathbf{r}) \rho g(r), \quad (12)$$

with the density ρ. Therefore in principle the structure factor contains the same information as the pair correlation function. However, due to numerical reasons and our implementation of shear boundary conditions it is easier to observe the long-range structure in the structure factor than in the pair correlation function. For our evaluation it is important that in a finite system $\mathbf{k}$ vectors are restricted to discrete vectors $2\pi \left(\frac{n_x}{L_x}, \frac{n_y}{L_y}, \frac{n_z}{L_z} \right)$ with $L_{x,y,z}$ being the system size in the x, y, and z directions and $n_{x,y,z} \in \mathbb{Z}$. We evaluate $S(\mathbf{k})$ for these $\mathbf{k}$ vectors and use $|S(\mathbf{k})|$ for further analysis. Since we do not evaluate the anisotropy of the structure factor in this study, we average over all possible orientations of the $\mathbf{k}$ vector. We sort the absolute values of the $\mathbf{k}$ vectors into intervals and average within these intervals over the values of the structure factors. Let us now discuss some typical features of the structure factor, corresponding to typical length scales present in the system.

One typical length for dense systems is about one particle diameter, the distance particle centers have to keep so that they do not overlap. The corresponding peak of the structure factor is the nearest-neighbor peak at $k = \frac{2\pi}{d}$. In a single crystal the peak would be sharp, since the particle positions are well defined, whereas in our case of a suspension there is a certain disorder, which broadens the peak.

Similar to the nearest-neighbor peak another peak can be detected at twice the $\mathbf{k}$ vector, which corresponds to a distance of one particle radius. This does not necessarily mean that there are particles whose centers are only one particle radius apart. It only means that for a certain $\mathbf{k}$ vector the addends in Eq. (11) do not cancel out each other.

For small $\mathbf{k}$ vectors there is another peak, or in our case an increase of the structure factor towards low $\mathbf{k}$ vectors. The length scale corresponds to the size of the whole system. If large clusters are formed, this can be seen in an increase of the low-$\mathbf{k}$ peak, since the contributions on this length scale do not cancel out each other anymore.

As already mentioned, later in this paper we focus on the low-$\mathbf{k}$ peak which corresponds to a length scale of the size of the system.

IV. SIMULATION SETUP

In this study the colloidal particles are represented by three dimensional spheres of $d = 0.37$ μm in diameter. This is the mean diameter of the particles used in the experiments to which we refer in Ref. [23]. We have simulated a small volume, $24d = 8.88$ μm long in the x direction, which is the shear direction, and $12d = 4.44$ μm long in the y and z directions. We have varied the volume fraction between $\Phi = 10\%$ (660 particles) and $\Phi = 40\%$ (2640 particles). Most of the simulations were performed at $\Phi = 35\%$ (2310 particles). We use periodic boundaries in the x and y directions and closed boundaries in the z direction [23]. Shear is applied in the x direction by moving small zones of particles and fluid close to the wall with a given shear velocity. The xy plane is our shear plane. For simulations without shear, to achieve the best comparability, we use the same boundary conditions and just set the shear rate to $\dot{\gamma} = 0$. In addition we have performed simulations with two different shear rates: with $\dot{\gamma} = 100/\text{s}$ and with $\dot{\gamma} = 500/\text{s}$. For better comparability to other works the Peclét number

$$\text{Pe} = 6\pi \eta R^3 \dot{\gamma} / k_B T, \quad (13)$$

which expresses the importance of Brownian motion with respect to the shear flow, is useful. The Peclét numbers in our shear simulations are Pe=3 and Pe=15, respectively.

V. RESULTS AND DISCUSSION

First, we focus on simulations without shear, where one can predict intuitively what should happen. Qualitatively the results are similar to our earlier work [22], but the quantitative relation between the pH value and the potentials is new. The relation was presented in Ref. [23], but here we apply it to different cases and we focus more on the characterization of the microstructure. However, given the particle-particle interaction potentials, the microstructure in equilibrium can be predicted easily, at least on a qualitative level. But, the matter changes and gets more sophisticated when shear is applied and an interplay between shear flow and particle-
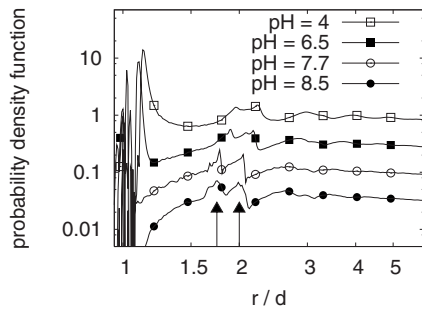
FIG. 1. Dependence of the particle correlation function on the pH value, $I=3$ mmol, $\dot\gamma=0/s$, $\Phi=35\%$. The plots for four different pH values are shifted against each other for better visibility by a factor of 3. For $pH=4$ the particles are not clustered. Hence the structure at $\frac{r}{d}=2$ is less sharp than in the other three curves of the plot and the nearest-neighbor peak (at $\frac{r}{d}=1$) is broad. For $pH=6.5$ slight clustering starts, the structures become sharper. For $pH=7.7$ strong cluster formation is reflected in very sharp structures. For $pH=8.5$ electrostatic repulsion nearly disappears so that no barrier between primary and secondary minimum exists anymore. The particles cannot rearrange anymore, and therefore the structures labeled by the arrows become smoothened compared to the case of $pH=7.7$.

particle interactions becomes responsible for the resulting microstructure.

A. Correlation function

For constant ionic strength $I=3$ mmol/l the local microstructure can be examined using the correlation function. Depending on the pH value the behavior of the system changes from a repulsive structure around $pH=4$ to a stable suspension around $pH=6$ towards a clustered region if the pH value is further increased, until the isoelectric point is reached at $pH=8.7$. There clustering occurs in any case, independent of the ionic strength. This can be seen in the structure of the correlation function: electrostatic repulsion prevents clustering (at $pH=4$). Particles are suspended, and there is no fixed long range ordering in the system. The correlation function (Fig. 1) shows a maximum at a typical nearest-neighbor distance slightly above $\frac{r}{d}=1$ with d denoting the particle diameter, then in the layer of next neighbors small correlations can be found (at $\frac{r}{d}=2$). For larger distances the correlation function is rather constant.

When the pH value is increased, the surface charge is lower, which at first causes the particles to approach each other more closely. The maximum of the correlation function is shifted to smaller distances (see Fig. 1, note that the curves are shifted vertically in the plot by a factor of 3 for better visibility). Then, van der Waals attraction becomes more important and clustering begins. One can see this in the correlation function where a sharp structure at particle distances between 1.5 and 2 particle diameters occurs. In a solidlike cluster the position of the next neighbor is fixed more sharply than in the suspension, consequently the nearest-neighbor peak becomes sharper, too, and its height is increased. Close to the isoelectric point ($pH=8.7$) the barrier between primary and secondary minimum disappears. The
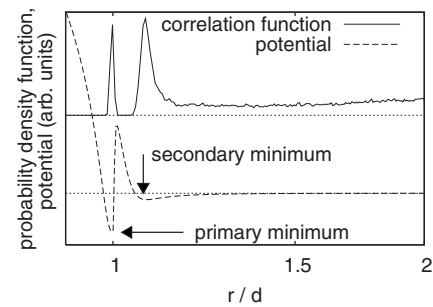

FIG. 2. Correlation function, $\dot\gamma=100/s$, $pH=7$, $I=3$ mmol/l, $\Phi=35\%$: one finds clustering in the primary and the secondary minimum. Note: The vertical axis is logarithmic, and a constant offset has been added before plotting. Thereby, the coincidence of the minima in the potential with the maxima in the correlation function becomes more apparent. The dotted lines denote the position of the base line before shifting.

particles, once clustered, cannot rearrange anymore, and therefore the correlations to the next neighbors become less sharp again (compare the cases of $pH=8.7$ and $pH=7.7$ in Fig. 1 at the positions denoted by the arrows).

Instead of varying the pH value, one can also vary the ionic strength to achieve similar effects. Increasing the ionic strength, experimentally speaking "adding salt" decreases the screening length $1/\kappa$ and therefore the attractive forces become more important: the particles start to form clusters. On the contrary, if the ionic strength is decreased—experimentally speaking a dialysis step is performed—the electrostatic repulsion prevents cluster formation and, for sufficiently strong repulsion, long range correlations occur as soon as the range of the repulsion reaches the mean particle distance.

In Fig. 2 one can see clustering in the primary minimum of the potential as well as in the very shallow secondary minimum. The correlation function plotted there is evaluated after 1000 SRD time steps in a simulation for $pH=7$ and $I=3$ mmol/l at a volume fraction of $\Phi=35\%$ sheared with $\dot\gamma=100/s$. Note that the shear flow is not of essential importance here, but it supports the particles to overcome the potential barrier between the primary and the secondary minimum. The dotted lines in Fig. 2 denote the zero line.

A secondary minimum only exists if the screening length of the electrostatic repulsion is short enough, i.e., if the ionic strength is large enough. According to the depth of the potential, clustering in the primary minimum is associated with much stronger forces than in the secondary minimum.

The effects described up to here can be observed with or without shear qualitatively in an analogous manner. If the suspension is sheared clustering occurs at higher pH values and the peaks found in the correlation function are slightly broadened, because the relative particle positions are less fixed. But a new feature appears, if a stable suspension of not too high volume fraction is sheared. Induced by the shear particles arrange themselves in layers. Regular nearest-neighbor distances in the shear plane cause the correlation function to become more structured even for large distances (see Fig. 3). The long range structure of the pair correlation function appears after a transient time the particles need to
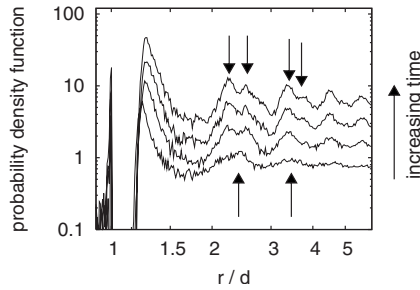
FIG. 3. Correlation function for $\dot{\gamma}=500/\mathrm{s}$, $p\mathrm{H}=6$, $I=0.3$ mmol/l, $\Phi=32\%$: depending on the simulation time the peaks indicated by the arrows from below split into two (indicated by the arrows from above), and long range correlations occur (for $\frac{r}{d}>4$). This reflects the process of layer formation and appearance of a regular (hexagonal) order in the layers. From bottom to top several states for increasing time are shown. The plots are shifted vertically by a factor of 2 for better visibility.

arrange themselves in the layered structure. The curves in Fig. 3 correspond to the same simulation, but for increasing time from bottom to top. The arrows from the bottom indicate the position of the next-neighbor peak and the next-but-one neighbors (since the particles do not touch each other, the peaks are located not exactly at $\frac{r}{d}=1,2,3,\ldots$). Within one layer which moves as a whole, a hexagonal particle order appears, which can be seen in the occurrence of a peak at $\frac{r}{d}=\sqrt{3}$ times the position of the nearest-neighbor peak, i.e., the next-neighbor peak splits, as indicated by the arrows from above. The same applies to the next-but-one-neighbor peak marked by the second set of arrows at $3<r/d<4$. Shear induced layer formation has been found in both experiments [49,50] and simulations [51–53].

We have integrated over the nearest-neighbor peaks both the peaks of the primary and the secondary minimum, and plotted the integral vs $p\mathrm{H}$ value in Fig. 4. We have chosen $I=3$ mmol/l and $\Phi=35\%$ and three different shear rates: $\dot{\gamma}=0$, 100, and 500/s. We have integrated the correlation function for $r<1.215d$, where for all $p\mathrm{H}$ values the potential in
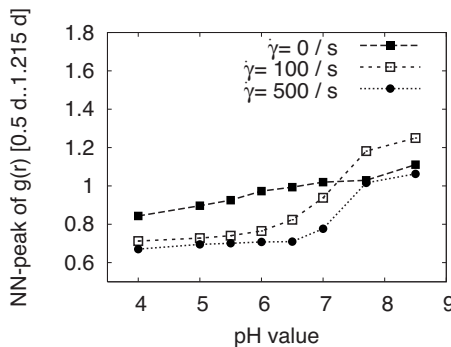

FIG. 4. Nearest-neighbor peak (primary and secondary minimum of the potential) of the correlation function $I=3$ mmol/l, $\Phi=35\%$: For low $p\mathrm{H}$ values clustering is prevented by the electrostatic repulsion. For high $p\mathrm{H}$ values the particles form clusters, which is reflected by an increased nearest-neighbor peak. First, shear prevents clustering, then depending on the shear rate, cluster formation takes place. Low shear rates even support cluster formation at high $p\mathrm{H}$ values.

the secondary minimum has a value of $-\frac{1}{2}k_BT$. In other words, we have captured the primary and the secondary minimum of the potential for this plot. For low $p\mathrm{H}$ values clustering (in the secondary minimum) is only possible for low shear rates. For high shear rates, the hydrodynamic forces do not allow the formation of stable clusters. For rising $p\mathrm{H}$ values the clustering increases, first for the unsheared suspension, at higher $p\mathrm{H}$ values for low shear rates ($\dot{\gamma}=100/\mathrm{s}$), and finally for high shear rates ($\dot{\gamma}=500/\mathrm{s}$). Remarkably, for $p\mathrm{H}>7.5$ the curve for $\dot{\gamma}=100/\mathrm{s}$ shows stronger cluster formation than the other ones. Particles are brought together by the shear flow, so that compared to the case of no shear, the clustering process is supported here. On the other hand, the shear stress may not be too strong, because otherwise the clustering process is limited by the shear flow again (for $\dot{\gamma}=500/\mathrm{s}$ the clustering is less pronounced than for $\dot{\gamma}=100/\mathrm{s}$).

B. Structure factor

The pair correlation function can be used to characterize the local order of the microstructure on the length scale of the particle size. However, to do the characterization on the length scale of the system size, we use the structure factor $S(\mathbf{k})$. In principle we could integrate the correlation function $g(r)$ over an interval for large r. However, due to our implementation of shear (see Ref. [23]), we have to close the boundary in the z direction. Therefore we already find restrictions for r around half the extension of the system in this direction. We find that it is easier to handle these finite size restrictions by moving on to the structure factor. There, we always find a low-$\mathbf{k}$ peak, even if no cluster formation takes place in the simulation. In contrast to experiments, where this peak only appears for clustered samples, it reflects the presence of a typical length of the system size in the simulation. Namely, the finite size of the simulation volume is the typical length, which appears in the structure factor by the low-$\mathbf{k}$ peak. This only produces a constant offset when integrating over the low-$\mathbf{k}$ peak as we are going to do below in this section. Thus it is easy to handle the influence of the finite system size in $\mathbf{k}$ space.

In Fig. 5 we have plotted several typical structure factors of our simulations. For these plots the $p\mathrm{H}$ value is fixed to $p\mathrm{H}=6$. Cases (a) and (b) are sheared with $\dot{\gamma}=500/\mathrm{s}$ at an ionic strength of $I=0.3$ mmol/l. In case (a) the volume fraction $\Phi=20\%$ is relatively low. Therefore the particles can arrange themselves in layers parallel to the shear plane, which move relatively independently in the shear flow. They have a certain distance fixed in space and time. This can be seen in a sharp peak at a dimensionless $\mathbf{k}$ vector of $k=5.2$, which corresponds to a distance of 1.2 particle diameters. In fact, this is exactly the distance between two neighboring layers, as one can easily verify by counting the layers in a snapshot of the system [Fig. 6(a)]. The particles in the layers do not have a fixed distance and therefore no second-order-peak can be observed.

For case (b) the volume fraction is increased to $\Phi=35\%$. The particle layers are packed more densely and therefore the interactions between one layer and the neighboring one
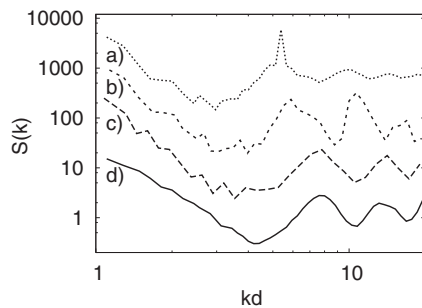
FIG. 5. Structure factor for some selected examples, with pH $=6$ fixed for all plots: $\dot{\gamma}=500/s$, $I=0.3$ mmol/l: (a) $\Phi=20\%$ and (b) $\Phi=35\%$; $\dot{\gamma}=0$, $I=25$ mmol/l: (c) $\Phi=40\%$ and (d) $\Phi=10\%$. The curves are shifted vertically for better visibility. In case (a) ten layers can be identified in the system, resulting in the strong peak close to 5. But, since the particles in the layers can still move freely, there is no second-order peak. In case (b) layers are formed, but particles are moving from one layer to the other, disturbing the flow. As a result the nearest-neighbor peak is much broader. Due to the structure in the layers, a second-order peak appears. In case (c) the interaction is strongly attractive, hence the particles approach each other and the nearest-neighbor peak is shifted to higher **k** vectors. In case (d) the volume fraction is much less. The slope of the low-**k** peak is much flatter, which depicts that the cluster is fractal.

become relevant. Particles jump from one layer to the other, which disturbs the flow and therefore the distance between the layers is not fixed anymore. The sharp peak on top of the nearest-neighbor peak disappears. Instead of that, in each layer a regular hexagonal order appears and therefore the second-order peak is much more pronounced.

In case (c) the ionic strength is increased to I $=25$ mmol/l. The interparticle potentials are attractive enough that aggregation takes place. In this simulation we did not apply shear, therefore one finds only one big cluster in the system [compare Fig. 6(c)]. In the cluster the particles are packed more densely and consistently the nearest-neighbor peak in the structure factor is shifted to larger **k** vectors. The volume fraction is $\Phi=40\%$ in this case.

In case (d) the volume fraction is decreased to $\Phi=10\%$. The particles still form clusters, but their mobility is not high enough to create one compact cluster. The system has a fractal structure [see Fig. 6(d)]. This can be seen in the structure factor as well: The slope of the low-**k** peak is flatter in this case compared to cases (a)–(c). A flatter slope of the low-**k** peak is typical for structure factors of fractal objects. The fractal dimension of the cluster extracted from the slope of the low-**k** peak is 2.5. In experiments this relation is often used to determine the fractal dimension of a sample: Lattuada *et al.* [54] have evaluated the fractal dimension of agglomerates of latex particles from the slope of the structure factor. McCarthy *et al.* [55] give an introduction to scattering intensities at fractal objects, without mentioning the structure factor, but their arguments refer to the contribution of the structure factor on the scattering intensity. The underlying mechanism which is responsible for these structures is cluster cluster aggregation [56].

In Fig. 7 we show the dependence of the low-**k** peak of the structure factor on the pH value. Here we have integrated
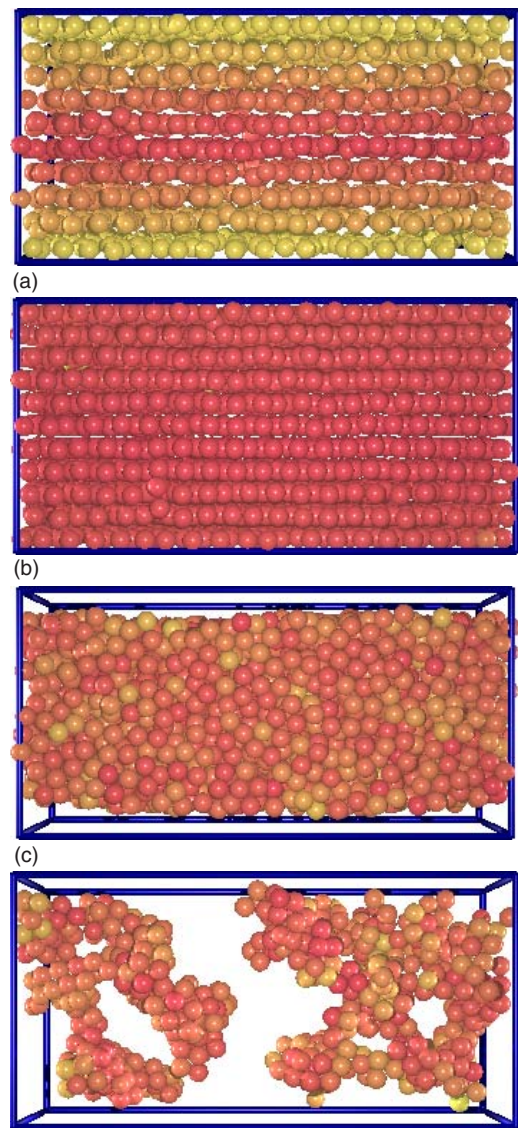

FIG. 6. (Color online) Snapshots of the systems analyzed in Fig. 5: In case (a) one can see the layers resulting in the sharp peak in the structure factor. In case (b) the layers are packed closer due to the higher volume fraction. Collisions between particles of neighboring layers happen more frequently. In case (c) one big cluster is formed. The particles are packed densely. In case (d) the fractal nature of the system can be seen directly.

over dimensionless **k** vectors smaller than 3 which means we have captured structures larger than twice a particle diameter. A large integral over the low-**k** peak is due to a large inhomogeneity in the system. In one part of the system particles are present and in the other part they are not. In other words, we observe the process of cluster formation on a length scale of the system size. Without shear, particles cluster in the secondary minimum for all pH values. If the system is slightly sheared ($\dot{\gamma}=100/s$) clustering is suppressed for low pH values. Starting at pH$=6$ cluster formation starts and is even supported by the shear flow for pH values larger than 7.5. For large shear rates ($\dot{\gamma}=500/s$) cluster formation is suppressed by the shear flow. By analyzing the low-**k** peak of the structure factor one observes on the length scale of the
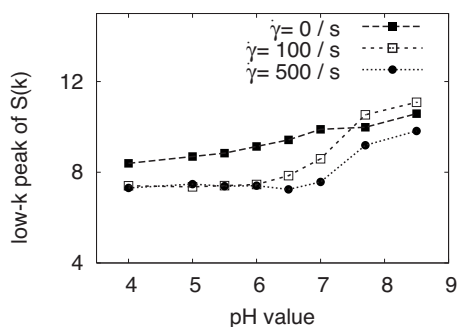
FIG. 7. Low-**k** peak for different pH values and different shear rates. The ionic strength I is kept constant at $I=3$ mmol/l and the volume fraction is always $\Phi=35\%$. For $\dot{\gamma}=0/$s the particles tend to cluster in the secondary minimum of the potential. This clustering can easily be broken up, if shear is applied. If the pH value is increased, shear cannot prevent cluster formation anymore. At low shear rates ($\dot{\gamma}=100/$s) clustering is even enhanced, since the particles are brought closer to each other by the shear flow. Note that the offset of the plots reflects the finite size of our system combined with the closed boundary conditions (see the text).

system size. The same behavior of the system can be seen by analyzing the pair correlation function, as we have already shown in Fig. 4. In that case one analyzes the number of nearest neighbors, that means one observes the length scale of a particle diameter. Nevertheless, both graphs show the same behavior of the system, i.e., we have a consistent picture of the cluster formation process on the length scale of the nearest neighbors and on the length scale of the system size.

Thus we have confirmed that the cluster formation process is not limited to length scales smaller than our system size. This is reflected especially by the transition between pH$=7-8$ and its shear rate dependence in the plots in Figs. 7 and 4. There is a strong similarity of the two plots, which are obtained by two evaluation methods referring to two different length scales. This confirms that the plots do not only reflect how clusters are formed on the respective length scale, but that the clustering process is a phenomenon which can be observed on *any* length scale by applying a suitable method to characterize it.

C. Density inhomogeneity

Another way to observe the cluster formation process is provided by the "demixing parameter" defined in Ref. [24] as follows: the system is divided into n^3 cubes and the particle density ρ_k is evaluated in each cube. Then the demixing parameter is the mean squared deviation of the density

$$\Psi_n = \sum_{k=0}^{n^3} (\rho_k - \bar{\rho})^2, \qquad (14)$$

where $\bar{\rho}$ is the mean density. For our elongated system we modify this definition and use $2n$ cubes in the x direction, resulting in $2n^3$ cubes in total. The demixing parameter implicitly contains information about the density of the clusters. It is the density fluctuation of the whole system. If the clus-
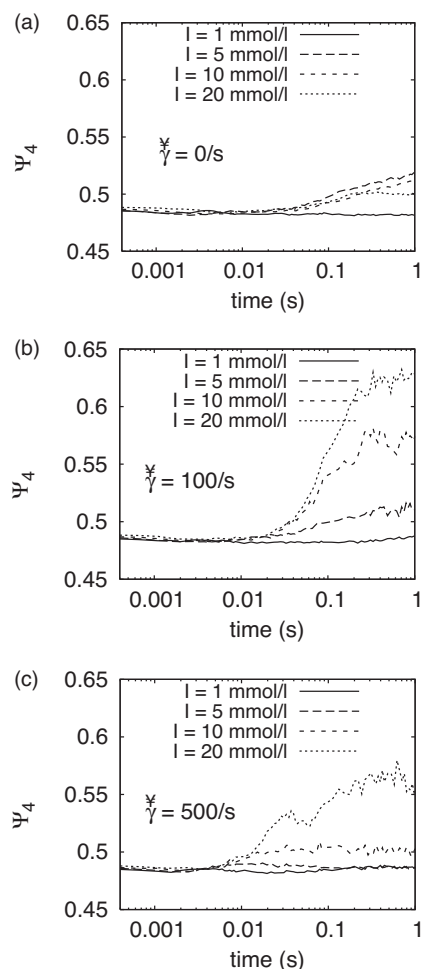

FIG. 8. Demixing parameter for constant pH$=6$ and volume fraction $\Phi=35\%$ for three different shear rates: $\dot{\gamma}=0/$s (a), $100/$s (b), and $500/$s (c). Without shear only very weak demixing takes place. For $\dot{\gamma}=100/$s the strongest demixing can be observed for the system with the highest ionic strength $I=20$ mmol/l. For lower ionic strengths the effect decreases until it disappears completely at $I=1$ mmol/l, where the repulsive regime is reached. If the shear rate is further increased ($\dot{\gamma}=500/$s), the clusters are less stable so that the system becomes less inhomogeneous. For $I=5$ mmol/l the demixing is even suppressed completely.

ters are more compact, voids have to appear and the demixing parameter increases, since the distribution of the local density is broadened thereby.

In Fig. 8 we have plotted the demixing parameter Ψ_4 vs time for three different shear rates and four different ionic strengths in each plot. The pH value is kept constant at pH $=6$ and the volume fraction at $\Phi=35\%$. Without shear Ψ_4 is nearly constant. Even if a cluster is formed, it does not move, so that the average density in the boxes does not change much. For lower volume fractions the time dependence without shear is stronger. If shear is applied the clusters are deformed so that stronger inhomogeneities appear. Depending on the ionic strength the demixing parameter increases with cluster formation (high ionic strength) or still stays constant when the interactions are repulsive (low ionic strength). For $\dot{\gamma}=100/$s the strongest cluster formation is achieved for the highest ionic strength $I=20$ mmol/l. If the ionic strength is
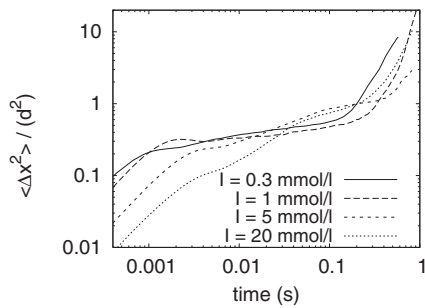
FIG. 9. Mean squared displacement at $pH=6$ for different ionic strengths, without shear. One can see a ballistic regime for short times, a central plateau and a collective long time movement which can be a movement of a whole cluster or cage escape events of single particles. Depending on the ionic strength, the central plateau is more or less pronounced. A comparison of the plateau for different simulations can be used to decide, if a certain state belongs to the repulsive region of the stability diagram. A state well in the liquid microstructure should be used as a reference for the comparison.

decreased, the clustering effect decreases as well, until it disappears completely at $I=1$ mmol/l, where the repulsive regime is reached. To see the shear rate dependence, compare the plots for $\dot{\gamma}=100/s$ and $500/s$. If the shear rate is increased, the cluster formation starts faster because the shear flow brings the particles faster in contact, but the resulting inhomogeneity of the final state is less than for lower shear rates. This effect can be seen in Fig. 4 and in Fig. 7, too. There, also the intensity of the respective peaks for $\dot{\gamma}=500/s$ is less than for $\dot{\gamma}=100/s$. This shows again that large shear rates can inhibit cluster formation, whereas moderate shear rates can support the clustering process [the plots in Fig. 8(b) for $\dot{\gamma}=100/s$ are steeper than the ones in Fig. 8(a) for $\dot{\gamma}=0/s$]. In addition to the information already contained in other quantities we have presented, Fig. 8 shows the time evolution. One can see three regimes of time evolution: for very short times all plots are nearly constant. This means that the cluster formation has not yet started. Then, the plots for attractive potentials rise, which shows the onset of cluster formation. For large times the slope of the plots decreases, which reflects that the clusters have been formed and no more "demixing" takes place. Without shear [see Fig. 8(a)], it is remarkable that for the largest ionic strength the growth of the demixing parameter first becomes constant after 0.3 s, whereas for the other cases where clustering occurs, it grows further. This reflects that in the case of $I=20$ mmol/l the attraction is that strong that no reordering of the particles is possible anymore.

D. Repulsive regime

To characterize the repulsive regime, we evaluate the mean squared displacement for the particles. In Fig. 9 we plot the mean squared displacement for different ionic strengths. The pH value is kept constant at $pH=6$ and the volume fraction is $\Phi=35\%$ for this plot. Three different regimes can be identified. For very short times, the ballistic regime, particles move on short distances without a notable
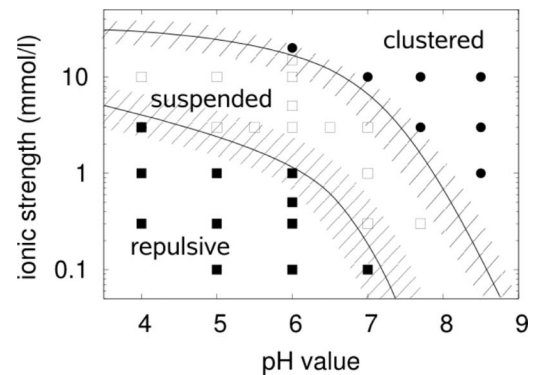

FIG. 10. Stability diagram (plotted for $\Phi=35\%$ and without shear) depicting three regions: a clustered region (filled circles), a suspended regime (open squares), and a repulsive structure (filled squares). In the clustered region particles aggregate which leads to inhomogeneity in the system. In the suspended regime, the particles are distributed homogeneously in the system and they can move freely. In the repulsive regime the mobility of the particles is restricted by electrostatic repulsion exerted by their neighbors. As a result they arrange in a local order which maximizes nearest-neighbor distances. The borders between the regimes are not sharp. They depend on the shear rate and on the volume fraction. Therefore we have indicated the crossover regions by the shaded patterns. The lines are guides to the eye.

influence by their neighbors. The distances are in the order of some percent of the particle diameter and the times are a few SRD time steps. For larger times the particles interact with their neighbors and therefore their mobility is limited due to collisions with the neighbors. This is reflected in the mean squared displacement by a plateau of reduced slope, which is more pronounced the more the mobility of the particles is restricted. For even larger time scales collective motion starts, i.e., clusters or groups of particles move, or single particles can escape from a cage formed by its neighbors. Depending on the ionic strength different effects are important and thus the shape of the curve is different. For large ionic strengths the particles form clusters and these clusters may drift or rotate in the system. Then the collective motion is more dominant and the mean squared displacement grows faster than in single particle diffusion. The mean squared displacement does not show a plateau, then. But in the repulsive regime, the neighbors limit the motion of the particles, and the slope of the plateau is flatter, i.e., the plateau is even more pronounced, compared to the suspended case. In the repulsive regime the particles tend to arrange themselves in layers when shear is applied [23] and long range correlations can be found in unsheared systems [22].

E. Stability diagram

The results of the investigations presented in this paper can be summarized in a stability diagram for our Al_2O_3 suspension (Fig. 10). Three different microstructures can be identified: a repulsive structure, a suspended region, and a clustered region. In contrast to our previous work [22,23], we have explored the parameter space more in the repulsive regime and deeper in the clustered region. We use the mean

squared displacement, the demixing parameter Ψ [24], the correlation function, and the structure factor to decide to which of the three microstructures a certain point in the stability diagram belongs. However, the borders between the regions are not sharp and they depend on the shear rate. We have indicated the crossover regions by the shaded patterns in the stability diagram. If the volume fraction is decreased, the region of the repulsive structure becomes smaller.

To decide if a state is in the suspended region or in the repulsive one of the stability diagram, we have compared the plots of the mean squared displacement for the simulations without shear. If the plateau was pronounced there, we have counted the state among the repulsive regime. As a second criterion one can compare the pair correlation function. If there are long range correlations even though the system is not sheared, then the microstructure is the repulsive one. Finally, the shear force can be used to localize the border to the repulsive regime. For a given shear rate and a fixed volume fraction, the shear force depends on the particle interactions. If the shear force increases compared to a state well in the suspended regime, the motion of the particles is blocked by the electrostatic interaction in the repulsive regime.

As we have mentioned in Sec. III, without shear weak clustering can be seen in the suspended case as well, since there is no barrier for the particles to enter the secondary minimum of the DLVO potential, but the clusters can be broken up again very easily. Thus to decide if a state belongs to the clustered or to the suspended regime, we first study the snapshots of the system. If we see no clusters there, the clustered regime can be excluded. But, if we see clusters, we next check the density of the clusters and the onset time of the increase of the demixing parameter Ψ, which is a measure for the time it takes to form clusters. Both the density and the time are indications for the stability of the clusters. If they grow slowly and their density is low, we count the state to the suspended regime. The demixing parameter Ψ shown in Fig. 8 implicitly contains information about the density of the clusters. It is the density fluctuation of the whole system. If the clusters are more compact, voids have to appear and the demixing parameter increases, since the distribution of the local density is broadened thereby. The stability diagram obtained by these criteria is consistent with the results of the simulations with shear flow, shown in Figs. 4 and 7. Especially, the increased cluster formation for $I=3$ mmol/l starting between pH=7 and 8 is reflected in an increased nearest-neighbor peak in Fig. 4, and low-**k** peak in Fig. 7, respectively, and in a border between suspended and clustered regime in Fig. 10. The repulsive structure for pH=4 and $I=3$ mmol/l cannot be recognized in Figs. 4 and 7, but in a pronounced layer formation.

VI. SUMMARY AND OUTLOOK

We have simulated colloidal particles in shear flow and investigated how the clustering process due to attractive DLVO potentials is affected by the hydrodynamic forces. We find a consistent behavior on different length scales. The nearest-neighbor peak of the pair correlation function has been used to observe the direct neighborhood of the particles and the low-**k** peak of the structure factor to keep track of the length scales up to the system size. In both cases a suppression of the cluster formation by the shear flow can be seen at low pH values. For large pH values low shear rates even support the clustering process. In contrast, for high shear rates it suppresses the cluster formation. We have evaluated the mean squared displacement and the demixing parameter Ψ [24] in order to draw the stability diagram as given in Fig. 10. To our knowledge this stability diagram for Al_2O_3 suspensions is reproduced quantitatively for the first time from simulations. It helps to predict the behavior of a real suspension. Our findings on the cluster formation process suggest that soft stirring can enhance the cluster formation in industrial processing of this material. Further investigations can be carried out on the fractal dimension and its dependence on the experimental conditions. The low-**k** peak of the structure factor can be used for that. The cluster size distribution could as well deliver interesting insights useful to design industrial processes. Apart from that one can apply our algorithm to different materials. To do so, one has to change the interaction constants and especially for the electrostatic repulsion the calibrations we have presented in Ref. [23] are necessary. We expect that the stability diagram does not change qualitatively, but the position of the borders will be different.

ACKNOWLEDGMENTS

[1] A. J. C. Ladd, J. Fluid Mech. **271**, 285 (1994).

[2] A. J. C. Ladd, J. Fluid Mech. **271**, 311 (1994).

[3] T. N. Phung, J. F. Brady, and G. Bossis, J. Fluid Mech. **313**, 181 (1996).

[4] L. E. Silbert, J. R. Melrose, and R. C. Ball, Phys. Rev. E **56**, 7067 (1997).

[5] K. Geoffrey Soga, John R. Melrose, and Robin C. Ball, J. Chem. Phys. **110**, 2280 (1999).

[6] L. Harnau and S. Dietrich, Phys. Rev. E **69**, 051501 (2004).

[7] E. J. W. Vervey and J. T. G. Overbeek, *Theory of the Stability*

of Lyophobic Colloids (Elsevier, Amsterdam, 1948).

[8] B. V. Derjaguin and L. D. Landau, Acta Physicochim. URSS **14**, 633 (1941).

[9] S. Alexander, P. M. Chaikin, P. Grant, G. J. Morales, P. Pincus, and D. Hone, J. Chem. Phys. **80**, 5776 (1984).

[10] M. J. Grimson and M. Silbert, Mol. Phys. **74**(2), 397 (1991).

[11] René van Roij and J.-P. Hansen, Phys. Rev. Lett. **79**, 3082 (1997).

[12] J. Dobnikar, Y. Chen, R. Rzehak, and H. H. von Grünberg, J. Phys.: Condens. Matter **15**, S263 (2003).

[13] V. Trappe, V. Prasad, L. Cipelletti, P. N. Segre, and D. A. Weitz, Nature (London) **411**, 772 (2001).

[14] Y. Levin, T. Trizac, and L. Bocquet, J. Phys.: Condens. Matter **15**, S3523 (2003).

[15] A.-P. Hynninen, M. Dijkstra, and R. van Roij, Phys. Rev. E **69**, 061407 (2004).

[16] A. de Candia, E. del Gado, A. Fierro, N. Sator, and A. Coniglio, Physica A **358**, 239 (2005).

[17] J. Dobnikar, R. Rzehak, and H. H. von Grünberg, Europhys. Lett. **61**, 695 (2003).

[18] T. Palberg, W. Mönch, F. Bitzer, R. Piazza, and T. Bellini, Phys. Rev. Lett. **74**, 4555 (1995).

[19] R. Yamamoto, K. Kim, Y. Nakayama, K. Miyazaki, and D. R. Reichman, e-print arXiv:cond-mat/0604404.

[20] R. Oberacker, J. Reinshagen, H. von Both, and M. J. Hoffmann, in *Ceramic Processing Science VI*, edited by N. Claussen, S. Hirano, and G. L. Messing (American Ceramic Society, Westerville, OH, 2001), Vol. 112, pp. 179–184.

[21] J. Reinshagen, R. C. D. Cruz, R. Oberacker, and J. Hoffmann (unpublished).

[22] Martin Hecht, Jens Harting, Thomas Ihle, and Hans J. Herrmann, Phys. Rev. E **72**, 011408 (2005).

[23] Martin Hecht, Jens Harting, Markus Bier, Jörg Reinshagen, and Hans J. Herrmann, Phys. Rev. E **74**, 021403 (2006).

[24] A. M. Puertas, M. Fuchs, and M. E. Cates, Phys. Rev. E **67**, 031406 (2003).

[25] M. Hütter, Ph.D. thesis, Swiss Federal Institute of Technology, Zurich, 1999.

[26] L. Bocquet, E. Trizac, and M. Aubouy, J. Chem. Phys. **117**, 8138 (2002).

[27] M. Smoluchowski, Bull. Int. Acad. Sci. Cracovie **8**, 182 (1903).

[28] M. P. Allen and D. J. Tildesley, *Computer Simulation of Liquids* (Oxford Science Publications, Clarendon Press, Oxford 1987).

[29] J. F. Brady and G. Bossis, Annu. Rev. Fluid Mech. **20**, 111 (1988).

[30] J. F. Brady, J. Chem. Phys. **99**, 567 (1993).

[31] A. Sierou and J. F. Brady, J. Fluid Mech. **448**, 115 (2001).

[32] A. Sierou and J. F. Brady, J. Fluid Mech. **506**, 285 (2004).

[33] M. Hütter, J. Colloid Interface Sci. **231**, 337 (2000).

[34] A. J. C. Ladd and R. Verberg, J. Stat. Phys. **104**, 1191 (2001).

[35] A. Komnik, J. Harting, and H. J. Herrmann, J. Stat. Mech.: Theory Exp. P12003 (2004).

[36] Y. Inoue, Y. Chen, and H. Ohashi, J. Stat. Phys. **107**, 85 (2002).

[37] J. T. Padding and A. A. Louis, Phys. Rev. Lett. **93**, 220601 (2004).

[38] A. Malevanets and R. Kapral, J. Chem. Phys. **110**, 8605 (1999).

[39] A. Malevanets and R. Kapral, J. Chem. Phys. **112**, 7260 (2000).

[40] M. Ripoll, K. Mussawisade, R. G. Winkler, and G. Gompper, Europhys. Lett. **68**, 106 (2004).

[41] R. G. Winkler, K. Mussawisade, M. Ripoll, and G. Gompper, J. Phys.: Condens. Matter **16**, S3941 (2004).

[42] I. Ali, D. Marenduzzo, and J. M. Yeomans, J. Chem. Phys. **121**, 8635 (2004).

[43] M. Ripoll, R. G. Winkler, and G. Gompper, Phys. Rev. Lett. **96**, 188302 (2006).

[44] M. Ripoll, K. Mussawisade, R. G. Winkler, and G. Gompper, Phys. Rev. E **72**, 016701 (2005).

[45] T. Ihle and D. M. Kroll, Phys. Rev. E **67**, 066705 (2003).

[46] T. Ihle and D. M. Kroll, Phys. Rev. E **67**, 066706 (2003).

[47] J. T. Padding and A. A. Louis, Phys. Rev. E **74**, 031402 (2006).

[48] E. Falck, J. M. Lahtinen, I. Vattulainen, and T. Ala-Nissila, Eur. Phys. J. E **13**, 267 (2004).

[49] B. J. Ackerson and P. N. Pusey, Phys. Rev. Lett. **61**, 1033 (1988).

[50] B. J. Ackerson, C. G. DeKruif, N. J. Wagner, and W. B. Russel, J. Chem. Phys. **90**, 3250 (1989).

[51] J. R. Melrose and D. M. Heyes, J. Chem. Phys. **98**, 5873 (1993).

[52] Alan A. Catherall, John R. Melrose, and Robin C. Ball, J. Rheol. **44**, 1 (2000).

[53] I. Cohen, T. G. Mason, and D. A. Weitz, Phys. Rev. Lett. **93**, 046001 (2004).

[54] M. Lattuada, H. Wu, and M. Morbidelli, Phys. Rev. E **64**, 061404 (2001).

[55] D. W. McCarthy, J. E. Mark, and D. W. Schaefer, J. Polym. Sci., Part B: Polym. Phys. **36**, 1167 (1998).

[56] K. Geoffrey Soga, John R. Melrose, and Robin C. Ball, J. Chem. Phys. **108**, 6026 (1998).